Distributed ice thickness and glacier volume in southern South America

Jonathan L. Carrivick[1*], Bethan J. Davies[2], William H.M. James[1]
Duncan J. Quincey[1] and Neil F. Glasser[3]

[1]School of Geography, University of Leeds, Woodhouse Lane, Leeds, West Yorkshire, LS2 9JT, UK.
[2]Centre for Quaternary Research, Department of Geography, Royal Holloway, University of London, Egham, Surrey, TW20 0EX, UK.
[3]Centre for Glaciology, Department of Geography and Earth Sciences, Aberystwyth University, Aberystwyth, Ceredigion, SY23 3DB, UK.

*correspondence to:
Email: j.l.carrivick@leeds.ac.uk
Tel.: 0113 343 3324

Abstract

South American glaciers, including those in Patagonia, presently contribute the largest amount of meltwater to sea level rise per unit glacier area in the world. Yet understanding of the mechanisms behind the associated glacier mass balance changes remains unquantified partly because models are hindered by a lack of knowledge of subglacial topography. This study applied a perfect-plasticity model along glacier centre-lines to derive a first-order estimate of ice thickness and then interpolated these thickness estimates across glacier areas. This produced the first complete coverage of distributed ice thickness, bed topography and volume for 617 glaciers between 41°S and 55°S and in 24 major glacier regions. Maximum modelled ice thicknesses reach 1631 m ± 179 m in the South Patagonian Icefield (SPI), 1315 m ± 145 m in the North Patagonian Icefield (NPI) and 936 m ± 103 m in Cordillera Darwin. The total modelled volume of ice is 1234.6 km^3 ± 246.8 km^3 for the NPI, 4326.6 km^3 ± 865.2 km^3 for the SPI and 151.9 km^3 ± 30.38 km^3 for Cordillera Darwin. The total volume was modelled to be 5955 km^3 ± 1191 km^3, which equates to 5458.3 Gt ± 1091.6 Gt ice and to 15.08 mm ± 3.01 mm sea level equivalent (SLE). However, a total area of 655 km^2 contains ice below sea level and there are 282 individual overdeepenings with a mean depth of 38 m and a total volume if filled with water to the brim of 102 km^3. Adjusting the potential SLE for the ice volume below sea level and for the maximum potential storage of meltwater in these overdeepenings produces a maximum potential sea level rise (SLR) of 14.71 mm ± 2.94 mm. We provide a calculation of the present ice volume per major river catchment and we discuss likely changes to southern South America glaciers in the future. The ice thickness and subglacial topography modelled by this study will facilitate future studies of ice dynamics and glacier isostatic adjustment, and will be important for projecting water resources and glacier hazards.

Keywords sea level equivalent; sea level rise; Patagonia; South America; subglacial topography; overdeepening; hypsometry

Highlights

- New outlines and new centrelines for 617 glaciers between 41°S and 55°S
- Ice thickness statistics and ice volume per glacier reported
- Ice below sea level and within overdeepenings quantified
- Ice volume per major hydrological catchment determined

Introduction and rationale

The southern South America glaciers and Patagonian Icefields (Figure 1) are sensitive to climate change due to their relatively low latitude location, low-elevation termini and rapid response times (Oerlemans and Fortuin, 1992). They are the largest temperate ice masses in the Southern Hemisphere outside Antarctica and are sustained by the large volume of orographic precipitation that falls over the Andes under the prevailing Westerly winds (Carrasco et al., 2002; Casassa et al., 2002). Most of these ice masses are presently experiencing a negative mass balance, especially tidewater and lacustrine-terminating glaciers, but some glaciers, such as Pio XI, Moreno and Garibaldi, are presently displaying a positive mass balance (Schaefer et al., 2015). The general and dominant trend of ice mass loss is manifest in pronounced glacier recession (Davies and Glasser, 2012) and the largest contribution to sea level rise per unit area in the world (Ivins et al., 2011; Mouginot and Rignot, 2015; Willis et al., 2012). Indeed this sea level contribution is ~ 10 % of that from all glaciers and ice caps worldwide (Rignot et al., 2003). Over the next two centuries, mass loss from these glaciers has implications for sea level rise (Braithwaite and Raper, 2002; Gardner et al., 2013; Glasser et al., 2011; Levermann et al., 2013), for increased hazards from glacial lake outburst floods (Anacona et al., 2014; Dussaillant et al., 2009; Harrison et al., 2006; Loriaux and Casassa, 2013), and for water resources.

Recent analysis of southern South America glaciers has yielded data regarding glacier area, areal and volume change since the Little Ice Age (LIA) (Davies and Glasser, 2012; Glasser et al. 2011), ice surface velocity (Rivera et al., 2012; Jaber et al., 2013; Mouginot and Rignot, 2015), surface mass balance (Koppes et al., 2011; Mernild et al., 2015; Schaefer et al., 2015; Willis et al., 2011) and surface thinning and elevation changes (dh/dt) (Rivera et al., 2007; Willis et al., 2012). These analyses are largely reliant on satellite observations due to the inherent difficulties in accessing large parts of the ice surface (cf. Paul and Mölg, 2014). There are few in situ observations (the few examples include Gourlet et al., 2016; Rivera and Casassa, 2002, and they target only the NPI and SPI) and none that cover all glaciers at a catchment-scale across the NPI, SPI, Cordillera Darwin,

Grand Campo Nevado and outlying small glaciers and icefields. As a result, directly observed data on bed topography and ice thicknesses are sparse. Yet, these data are essential for calculations of ice volume, potential sea level contribution, and are a key input parameter in numerical modelling studies (Huybrechts, 2007), particularly when it is the smaller outlying glaciers and icefields with fast response times that will respond most rapidly to climate change (Meier, 2007; Raper and Braithwaite 2009). This study aims to provide the first complete regional calculation and assessment of distributed glacier ice thickness and catchment-scale ice volume of all southern South America glaciers (Figure 1).

Southern South America: ice fields and volcanoes

Our study area extends along the axis of the Andean mountain chain from Isla Hoste at 55 °S to Parque Nacional Vicente Perez Rosales at 41°S (Figure 1). The highest peaks nearly reach 4000 m.asl and the terrain is generally steep. The area is characterised by a highly maritime climate with a pronounced east-west precipitation gradient (cf. Figure 1), influenced by the westerly airflow over the Andes (Aravena and Luckman, 2009; Garreaud et al., 2009). The steep orographically-driven precipitation gradient produces precipitation on the western side of the Andes that is 100 % to 300 % higher than on the eastern side. At 49 °S the precipitation totals are 7220 $mm.yr^{-1}$ east of the Andes, and 209 $mm.yr^{-1}$ at Lago Argentino on the western side. Firn cores on the NPI confirm the east-west gradient in accumulation (Rasmussen et al., 2007).

In Northern and Central Patagonia, precipitation has steadily decreased since around the 1960s (Aravena and Luckman, 2009). Garreaud et al. (2013) found a 300 mm to 800 mm per decade decrease in precipitation in north-central Patagonia, and a 200 mm to 300 mm per decade increase south of 50 °S, which may account for generally positive glacier mass balances south of 50^{o}S (Shaefer et al., 2015), decreasing rates of glacier recession south of 50 °S after 2001 and faster rates of recession north of 50 °S (cf. Davies and Glasser, 2012). There is also evidence of widespread air temperature warming in Patagonia (Garreaud et al., 2013). Warming of the upper atmosphere (850 hPa; ca. 1400 m.asl) has been ~0.5 °C from 1960 to 1999, both in winter and summer and this warming has caused a decreased in the amount of precipitation falling as snow and increased ablation, exacerbating glacier recession (Rasmussen et al., 2007).

Some of these changes in precipitation have been related to variations in the strength of the prevailing Southern Hemisphere Westerlies, with stronger westerlies augmenting local precipitation. Stronger westerlies will also result in a decreased amplitude of the local air temperature annual cycle,

while weaker westerlies result in a colder winter and warmer summer, increasing temperature seasonality (Garreaud et al., 2013). The core of the Southern Hemisphere Westerlies is currently 50 to 55°S, but through the Holocene latitudinal variations in these winds periodically brought increased precipitation to the area, driving glacier advance and recession (Boex et al., 2013; Lamy et al., 2010; Moreno et al., 2012) but with a pronounced east-west shift (Ackert et al., 2008).

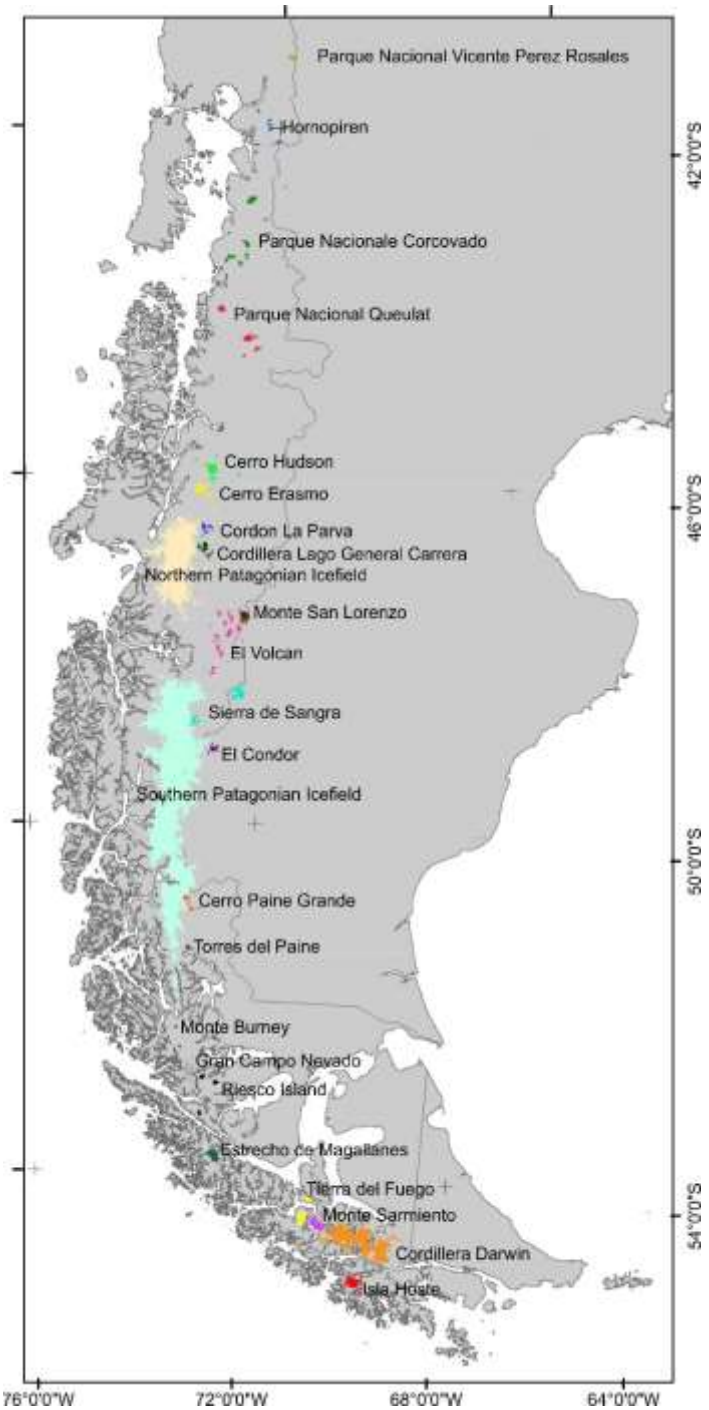

Figure 1. Southern South America with the 24 major glacier regions of this study displayed in unique colours.

The study area (Figure 1) includes 617 glaciers (mapped by Davies and Glasser, 2012; data available from the GLIMS database: http://nsidc.org/glims/). These glaciers are found predominantly within four key icefields: the North Patagonian Icefield (NPI), the South Patagonian Icefield (SPI), Gran Campo Nevado (Schneider et al., 2007) and Cordillera Darwin (Bown et al. 2014), but also on numerous outlying mountains and volcanoes (Rivera and Bown, 2013) (Figure 1).

In 2011, the total glacierised area of the study region was 22,717.5 km^2, with the SPI covering 13,218 km^2, the NPI covering 3,976 km^2, Cordillera Darwin covering 1832.7 km^2 and Gran Campo Nevado covering 236.9 km^2 (Davies and Glasser, 2012). The large western outlet glaciers of the SPI mostly extend down to sea level and calve into fjords, whilst those on the eastern slide largely terminate in large proglacial lakes (Warren and Sugden, 1993; Rasmussen et al., 2007). The NPI glaciers have mean elevations of 1000 m to 1500 m, with one glacier (San Rafael) terminating in a tidal lagoon, whilst the rest are lacustrine- or terrestrial-terminating glaciers. The ELA of outlet glaciers of the NPI ranges from ~700 m.asl on the west and 1200 m.asl on the east (Kerr and Sugden, 1994; Barcaza et al., 2009). Snowline mapping in the SPI suggested that ELAs ranged from ~800 m to 1400 m.asl (De Angelis, 2014).

Previous ice-thickness measurements in southern South America

Although the total ice area of the Patagonian Icefields is well constrained, the total ice volume is poorly known. Most studies have focused on surface elevation change (dh/dt) using digital elevation model (DEM) differencing, and from this have calculated glacier thinning and volume *change* (Rignot et al., 2003; Willis et al., 2011). Alternatively, researchers have applied volume-area scaling methods to estimate total ice volume (Grinsted, 2013), but this provides no data on bed topography and has been criticised for being applied inconsistently or too simplistically (Bahr et al., 2014) and because volume estimates are very sensitive to the scalar applied (Radic et al., 2008).

Glasser et al. (2011) estimated change in ice volume from the Little Ice Age (LIA) to present day by inferring palaeo-ice thicknesses from trimlines, moraines and other geomorphological data and by assuming a convex cross-valley ice surface profile at the LIA maximum. The change in ice volume was calculated by differencing shapefiles of LIA glacier extent and glacier extent in 2002. However, a lack of data on bed topography underneath present-day glaciers prevented the determination of present-day ice volume.

There are just fourteen spot measurements of ice thickness in South America (Gärtner-Roer et al., 2014). Distributed bed elevation and hence ice thickness data are available for some parts of the Southern Patagonia Icefield, as derived using a radio-echo sounding system (Rivera and Casassa, 2002). A gravity traverse in the 1980s suggested that there was up to 1.5 km of ice on the NPI (Casassa, 1987). Radar sounders have had little success, due to high absorption and scattering of radar in temperate ice. Ground radars have been limited to ice thicknesses of ~700 m to 750 m of ice (Raymond et al., 2005). Seismic measurements have indicated that Glaciar Moreno has a maximum depth of 720 m (Rott et al., 1998). More recently, helicopter-borne gravity observations have provided observations of ice thickness and bed topography across 49 % of the NPI and across 30 % of the SPI but have excluded all glaciers outlying from the icefields (Gourlet et al., 2016). This dataset is further limited in coverage because adverse weather during these helicopter surveys prevented the survey of Glaciar San Quíntin on the NPI and Glaciar Greve on the SPI.

Data sources and methods

DEM

We obtained an Advanced Spaceborne Thermal Emission and Reflection Radiometer Global Digital Elevation Model Version 2 (ASTER GDEM V2) mosaic from http://asterweb.jpl.nasa.gov/gdem.asp. ASTER GDEM V2 has a 30 m (1 arc-second) grid of elevation postings, with accuracies of 20 m for vertical data and 30 m for horizontal data at 95% confidence level.

Glacier outlines

Glacier drainage basins (Figure 2A) were obtained from Davies and Glasser (2012). They were mapped from orthorectified (level 1G) Landsat Enhanced Thematic Mapper Plus (ETM+) images from the year 2010-2011, which were pre-registered to the Universal Transverse Mercator (UTM) World Geodetic System 1984 ellipsoidal elevation (WGS84), zone 18S projection. These images have a spatial resolution of 30 m and a geopositional accuracy of ± 50 m (Davies and Glasser, 2012).

The drainage basins were edited to include nunataks and this new dataset we refer to herein as 'glacier outlines'. Nunataks, or areas of ice-free terrain, were identified in this study using Landsat 8 Operational Land Imager (OLI) scenes and a mask derived from the Normalised Difference Snow Index (NDSI = (Green – SWIR)/(Green + SWIR)). OLI scenes were selected to have been acquired during summer months (December-March) to minimise cloud, snow and shadow. Threshold values of the NDSI varied between 0.4 and 0.5, except for images covering Cordillera Darwin where persistent cloud-cover limited the available data to a single scene. In this case a value of 0.25 was

used to avoid the inclusion of deep shadow. Some minor manual editing of the automatically-derived nunataks was required to remove isolated pixels and pixel groups representing surface debris most commonly medial moraine, and some supraglacial lakes and some clouds. Despite this editing, and because we relied on a single Landsat scene per region, there is a chance that some nunataks were not include, and a chance that some erroneous nunataks persist.

Glacier centrelines

The identification of glacier ice-surface flow trajectories requires fully distributed velocity fields. These data are available for some of the outlet glaciers of the NPI and SPI (Jaber et al., 2014; Mouginot and Rignot, 2015), but are lacking for Cordillera Darwin, Gran Campo Nevado, and the numerous smaller outlet glaciers and icefields. The lack of a complete velocity dataset makes regional scale applications of automatic *flowline* generation unachievable (Kienholz et al. 2014).

Whilst manual digitization of *centrelines* is a subjective process and is time consuming in comparison to automatic extraction methods such as those using GIS hydrology tools (e.g. Schiefer et al., 2008; Machguth and Huss 2014), cost-distance analysis (e.g. Kienholz et al. 2014) and geometric analysis (e.g. Le Bris and Paul 2013), manual digitization is expert-driven. Unfortunately, our attempts to use these automatic centreline calculation methods on southern South America glaciers lead us to suggest that these automated techniques are also susceptible to edge cases and frequently fail to operate in glaciers with a complex or unusual form. Furthermore, all the aforementioned examples of automatic centreline extraction have been reported only in terms of method development and are not with freely-available code and not with full testing on a regional scale.

In this study, centrelines were manually digitized from the centre of a glacier terminus, propagating up-glacier approximately midway between and parallel to the lateral margins of any glacier ablation tongue, and thence towards any prominent saddles or cols on cirque headwalls or on ice divides (Figure 2A). In the same manner centrelines were created for each major glacier tributary (Figure 2A) to produce a total of 1,995 centrelines. To permit comparisons between this and past studies, and noting that our model mostly depends on ice surface slope, we did not make edits in the few cases where our glacier outlines or our glacier centrelines did not exactly match those from ice surface velocity analyses (Mouginot and Rignot, 2015).

Calculating ice thickness at points along the centreline

Ice thickness *h* of mountain glaciers can be estimated from a glacier surface slope α using a perfect plasticity approach by:

$$h = \frac{\tau_b}{fpg\ tan\ \alpha} \quad (1)$$

where τ_b, is basal shear stress and a shape factor *f* is required to account for valley sides supporting part of the weight of the glacier. In this study we used the ArcGIS tool developed by James and Carrivick (2016), which extended existing perfect plasticity models from application along single centrelines to fully 3D coverage, accommodated calculations on glaciers with complex geometry and automated this approach for application to multiple glaciers or whole glacier regions. Since that model is published (James and Carrivick, 2016) we simply cover the most salient points herein.

We calculated *h* at points spaced 50 m apart on all centrelines where that spacing was selected considering the 30 m resolution of the ice surface model and the spatial coverage of this study. Whilst *f* has been incorporated as a constant (usually 0.8 according to Nye 1965: e.g. Linsbauer, Paul and Haeberli 2012), Li et al. (2012) developed a more physically realistic method to dynamically adjust f depending on the local width of a glacier. In detail, Li et al. (2012) estimated ice thickness *perpendicular to the ice surface* but in this study we are dealing with GIS-analysed glacier geometry so to consider 'vertical' ice thickness, *h*, i.e. that *perpendicular to a horizontal x-axis* we re-write the Li et al. (2012) equation as:

$$h = \frac{0.9\ w(\frac{\tau_B}{pg\ tan\ \alpha})}{0.9\ w-(\frac{\tau_B}{pg\ tan\ \alpha})} \quad (2)$$

where *w* is half the glacier width at the specified point on a centreline.

Where nunataks are present, or where tributaries converge, Li et al. (2012) cautioned that this type of width calculation may be inaccurate. We therefore implemented an automatic check for erroneous values by: (i) checking if the perpendicular 'width' line intersected another centreline and (ii) cross checking if the resulting f value (Eq. 1) is realistic (> 0.445, equal to a half width to centreline thickness ratio of 1: Nye 1965). At points where either of these conditions were met, *h* was calculated using Eq. 1, with *f* set to that of the average of all points on the same tributary.

Interpolating distributed ice thickness and bed topography

Distributed ice thickness was interpolated from the centreline points across each glacier using the ANUDEM 5.3 interpolation routine, which is an iterative finite difference technique designed for the creation of hydrologically correct DEMs (Hutchinson 1989). ANUDEM generates preferably concave shaped landforms, thus mimicking the typical parabolic shape of (idealised) glacier beds (Linsbauer et al. 2009). It is commonly applied to estimating bed topography of both mountain valley glaciers (Farinotti et al., 2009; Li et al., 2012; Linsbauer et al., 2012; Fischer and Kuhn 2013) and ice sheets, such as within the Antarctica Bedmap2 dataset (Fretwell et al. 2013). In this study we forced the interpolation of ice thickness to zero at glacier outlines that were not in contact with another outline. Interpolations of ice thickness through ice divides was achieved simply by 'dissolving' (i.e. removing) those parts of glacier outlines that were in contact with each other.

Once thickness *h* for each grid cell in each glacier had been interpolated, total volume *V* was calculated:

$$V = \sum(c^2 h) \quad (3)$$

where c is the cellsize, which was 100 m.

James and Carrivick (2016) compared modelled (individual) glacier volume to that derived from field measurements of alpine glaciers around the world, and found worst-case 26.5 % underestimates and 16.6 % overestimates. For comparison errors for volume scaling approaches range from 30 % for large samples to 40 % when considering smaller (~ 200) samples (Farinotti and Huss 2013). Part of the model error in this study comes from the perfect-plasticity assumption, and part comes from the spatial interpolation from centreline thicknesses to glacier-wide thickness. Where James and Carrivick (2016) were able to compare centreline modelled thickness with thickness from field radar measurements on alpine glaciers around the world they found differences < 11 %. They also found that larger glaciers were least sensitive in terms of modelled volume to model parameters, which are described and explained in the next sub-section. Across southern South America 73 % of all glaciers are > 3 km^2 and > 96 % are of a mountain glacier type being underlain by high-relief subglacial bed topography that controls ice flow, so this an ideal study site in which to apply this model. In this study our uncertainty is spatially-variable and we therefore report modelled ice thickness with a mean uncertainty of ± 11 % and glacier volume with a mean uncertainty of ± 20 % but note that

these uncertainties will rise in the worst cases which are where there are large floating glacier terminii.

To estimate sea level equivalent ice volume was converted to a mass via an estimate of ice density. We used a single theoretical value for ice of 916.7 kg.m^{-3} and assigned this globally to the whole study area. We acknowledge that this does not consider snow or firn, which in some parts of southern South America where snow accumulation is very high could be volumetrically significant. For example, Schwikowski et al, 2013 drilled on Pio XI glacier and found ~ 50 m of snow/ firn (with densities < 800 kg.m^{-3}) and a similar ~ 50 m thickness of snow / firn was found on Tyndall glacier (Godoi et al., 2002). However, (i) these snow / firn depths account for ~ 10 % of the mean glacier thickness (as will be presented below) and (ii) we have no way of spatially-interpolating them either per glacier or for the whole of southern South America.

Parameterisation

The model employed in this study uses an ice surface DEM and glacier outlines to automatically derive glacier specific values of basal shear stress τ_b, slope averaging distance α_d, "effective width" slope threshold α_{lim}, and minimum slope threshold α_0, as explained below.

τ_b is variable between individual glaciers due to basal water pressure, ice viscosity and subglacial sediment deformation, for example (Cuffey and Patterson, 2010). For ice thickness estimations such as those within in this study, $\tau_b$does not have to be varied longitudinally for an individual glacier as a constant value can reproduce accurate thickness estimates along the length of a centreline (Li et al. 2012). Whilst τ_b can be "constrained reasonably from just a few ice-thickness measurements" (Li et al. 2012 p.7), in southern South America > 85 % of all glaciers do not have any ice thickness measurements, thus requiring τ_b to be estimated. Previous studies have used an empirical relationship between altitudinal extent and $\tau_b$that was developed by Haeberli and Hoelzle (1995) but the relationship is weak (r^2 = 0.44) and Linsbauer et al. (2012) reckoned an uncertainty of up to ± 45 % using this method. Therefore in this study we employ a relationship established by Driedger and Kennard (1986a), using area and slope in an elevation band approach:

$$\tau_b = 2.7 \cdot 10^4 \sum_{i=1}^{n} \left(\frac{A_i}{\cos \alpha_i}\right)^{0.106} \quad (4)$$

where the elevation band area (A_i) is in m^2 and τ_b is in Pa. This method was tested by Driedger and Kennard (1986b) as part of a volume estimation study, and they found a standard deviation of error of 5 % when comparing modelled with measured volumes. We calculated A_i and $\cos \alpha_i$ over 200 m ice-surface elevation bands to produce glacier specific average τ_b values that were consequently applied to each centreline point.

Reliable ice thickness *h*, estimates required analysis of the centreline gradient over an appropriate slope distance α_d. If α_d is too short small scale variations in the surface topography are produced in the estimated bed profile. Conversely, if α_d is too long, variations in the surface topography may be smoothed or omitted. Therefore α_d should be several times the local ice thickness (Paterson 1994). In this study we automatically set α_d to be 10 times the average ice thickness $\bar{h}$, with $\bar{h}$ derived from a volume area scaling approach (Radić and Hock 2010):

$$\bar{h} = \frac{0.2055A^{1.375}}{A} \quad (5)$$

where *A* is glacier area. This α_d also usefully served to virtually eliminate the effects of some small areas of 'noise' in the ice surface DEM, which is an unfortunate artefact inherent in the GDEM product especially over areas of low-angle ice and snow.

Using Eq. 2, *h* will tend to infinity as surface slope tends to zero, meaning *h* may be overestimated in regions of flatter ice surface (Li et al. 2012; Farinotti et al. 2009). In this study a 'minimum slope threshold' α_0 of 1.7° was used to re-assign any lower slope values to that minimum value. We note that Farinotti et al. (2009) used 5° and Li et al. (2012) used 4°, but since 40 % of the ice surface in southern South America is 4 or less this was too high a value for application to the glaciers of southern South America. Additionally, the 'low slope' parts of ice surfaces are generally situated within the trunks of the major outlet glaciers (and not to the 'plateau' itself which commonly has clearly discernible drainage basin divides marked by either a change in curvature between adjacent steep > 45 ° slopes or by nunataks). Only 0.5 % of the ice surface in this study is < 1.7°.

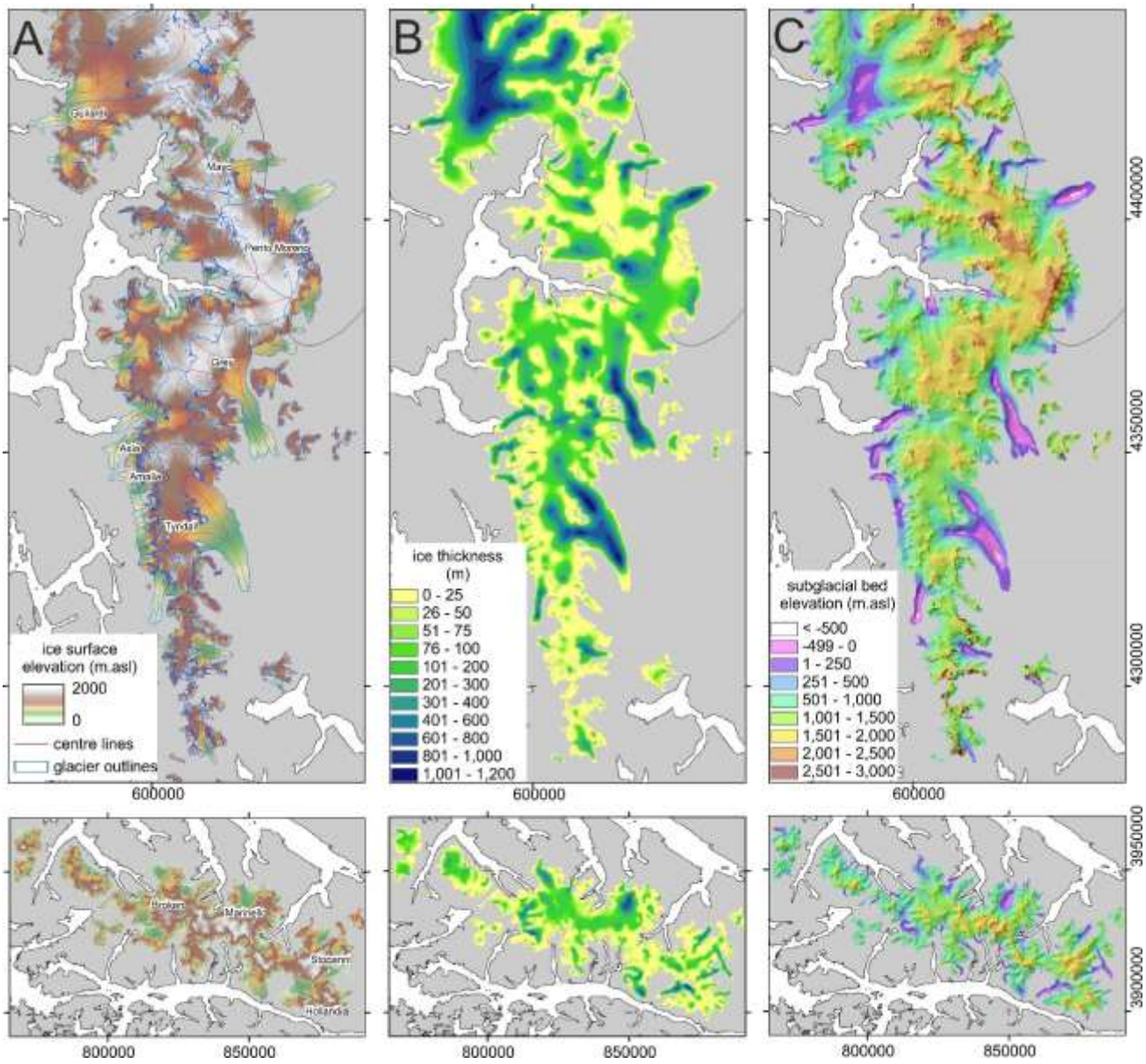

Figure 2. Examples from the southern part of the SPI (uppermost larger panels) and from the Cordillera Darwin region (lowermost smaller panels) of the Digital Elevation Model (DEM), glacier outlines and glacier centrelines (A), which together enabled modelling of distributed ice thickness (B) and thus bed topography (hillshaded in these images) (C). Only major glaciers are named in panel A for clarity. Both sets of panels have the same spatial scale and the same legends.

In this study we specified an 'effective width slope threshold' α_{lim} of 30°, so as to consider that where glaciers are thin valley walls contribute negligible support and thus in this situation should not be included in Eqn 2. This threshold of 30° represents *h* values of 27 m and 37 m as parameterised for the European Alps (130 kPa) and for the New Zealand Alps (180 kPa), respectively (Hoelzle et al. 2007) and is the optimal value found during analysis by Li et al. (2012). These *h* values are also

355 consistent with Driedger and Kennard (1986a) who found a threshold $\bar{h}$ ~36 m where glaciers obtain
356 a critical shear stress and contributed to ice deformation.
357
358 ***ELA estimation***
359 Glacier equilibrium line altitudes delineate a theoretical boundary between zones of net accumulation
360 and net ablation over multiple years. The inter-annual ELA fluctuates primarily due to changes in
361 weather and can be approximated by the end-of-summer snowline (EOSS). Across Patagonia
362 snowlines for 2002 to 2004 have only been measured via remote sensing for a few tens of SPI
363 glaciers by De Angelis et al. (2014) and for the period 1979 to 2003 for a few tens of NPI glaciers by
364 Bacaza et al. (2009). ELAs have also been modelled across southern South America via spatial
365 interpolation of continuous automatic weather station data from 1960 to 1990 by Condom et al.
366 (2007).
367
368 To extend analysis of ELAs across the whole of southern South America in this study, and mindful
369 of the lack of knowledge of mass balance gradients (c.f. Raper and Braithwaite, 2009), we used the
370 median elevation (Hmed) of glaciers as the most simple proxy for ELA, which was first proposed by
371 Hess (1893) and has been widely used since (e.g. Carrivick and Brewer, 2004; Braithwaite and
372 Raper, 2010; Davies and Glasser, 2012). We used Hmed as a proxy for ELA because we found
373 correlations between the published values of EOSS for both the NPI (r^2 = 0.72: Figure 3A) and for
374 the SPI (r^2 = 0.6: Figure 3B). The correlation of Hmed between the modelled ELA 1960 to 1990 of
375 Condom et al. (2007) is less strong (r^2 = 0.4: Figure 3C) and has a spatial pattern of increasing
376 discrepancy southwards (SI_A). We interpret this poorer correlation of Hmed with modelled ELA to
377 suggest that glacier geometry has responded significantly to climate change during the 20 years
378 between 1990 and our glacier outline inventory of 2010-2011 and thus that the modelled ELA of
379 Condom et al. (2007) is not a good representation of the contemporary ELA.
380

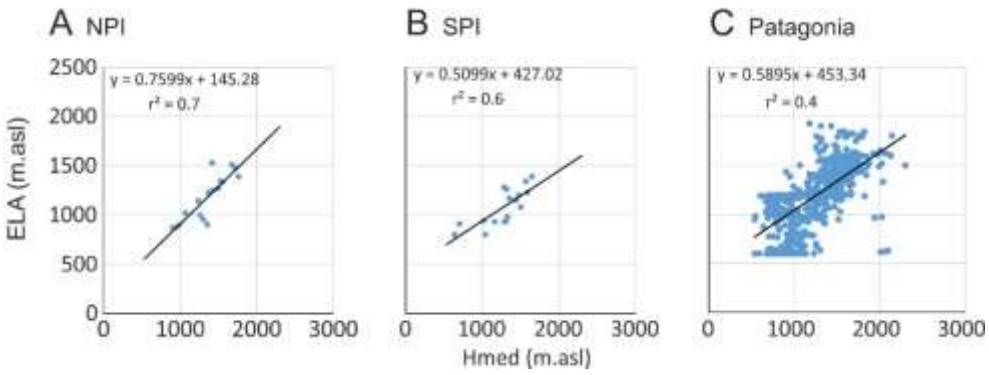

381

Figure 3. Comparison of ELAs estimated from end-of-summer snowlines with median glacier elevation (Hmed) for the NPI (A) and SPI (B). Note different that the snowlines for the NPI and for the SPI were measured over different time periods and by Barcaza et al. (2009) and by De Angelis et al. (2014), respectively. Comparison of the long-term ELA as modelled via spatial interpolation of climate data 1960 to 1990 by Condom et al. (2007) with Hmed of glaciers in the 2010-2011 glacier inventory (C).

Spatial and statistical analysis

Zonal statistics per glacier, per major glacial region and per major river catchment were extracted from ice-surface elevation, ice thickness, subglacial bed topography and ELA trend grids in ArcGIS. Bed elevations below sea level were automatically extracted via a binary reclassification of bed topography [> 0 m.asl = 0, < 0 m.asl = 1], conversion of the '1' values in this grid to polygons, and then zonal analysis of bed topography per polygon zone. Overdeepenings were automatically extracted from bed topography by 'filling sinks' in the bed topography and analysed in the same manner as for bed elevations. Major rivers and major lakes in southern South America were manually digitised in a GIS using Landsat images. River catchments that intersected glacier outlines were extracted from HydroSHEDS (Lehner et al., 2006), which is derived from elevation data of the Shuttle Radar Topography Mission (SRTM) at 90 m resolution.

Results

Overall, the 617 glaciers considered in this study cover an area of 22,121.9 km^2 with a mean thickness of 264 m and comprising a total volume of 5955 km^3 ± 1191 km^3**.** Using an ice density of 916.7 $kg.m^{-3}$, this volume equates to 5458.3 Gt ± 1091.6 Gt ice and to 15.08 mm ± 3.01 mm sea level equivalent (SLE).

There is a wide range in Hmed of glaciers within each major glacier region (Table 1), reflecting the strong precipitation and temperature gradients in the area and the controls of these upon glacier surface energy balance and glacier mass balance. The difference in mean Hmed value between each major glacier region (Table 1) is crudely associated with latitude with lower mean Hmed occurring farther south. A table of glacier geometry, ice thickness and volume attributes, per glacier, is included in supplementary information (SI_Table1).

Major glacier region	Mean ice thickness (m)	Max. ice thickness (m)	Volume (km^3)	Sea level equivalent (including ice mass below sea level) (mm)	Maximum potential sea level rise (excluding ice mass below sea level) (mm)	Minimum Hmed (m.asl)	Mean Hmed (m.asl)	Maximum Hmed (m.asl)
Gran Campo Nevado	79	639	19.7	0.05	0.05	537	841	1230
Cordon La Parva	33	379	2.6	0.01	0.01	1227	1547	1845
Northern Patagonian Icefield	305	1315	1234.6	3.13	3.10	904	1417	1809
Cerro Hudson	131	759	28.5	0.07	0.07	1259	1436	1594
Cerro Erasmo	107	871	14.9	0.04	0.04	1204	1429	1569
El Volcan	44	361	14.8	0.04	0.03	992	1529	1792
Cordillera Lago General Carrera	39	696	5.0	0.01	0.01	1490	1720	2299
Monte San Lorenzo	57	739	8.1	0.02	0.02	1340	1901	2131
Southern Patagonian Icefield	331	1649	4326.6	10.96	10.62	638	1242	2097
Sierra de Sangra	67	449	17.8	0.05	0.05	1416	1595	2026
Cordillera Darwin	82	936	151.9	0.38	0.37	602	950	1659
El Condor	50	552	3.8	0.01	0.01	1327	1435	1542
Isla Hoste	93	651	20.0	0.05	0.08	536	755	851
Monte Sarmiento	69	474	12.5	0.03	0.04	691	869	1141
Cerro Paine Grande	72	491	5.4	0.01	0.01	1056	1292	1537
Tierra del Fuego	63	379	9.9	0.03	0.02	664	770	814
Estrecho de Magallanes	222	845	39.9	0.10	0.10	404	724	976
Riesco Island	48	548	5.1	0.01	0.01	746	876	1071
Torres del Paine	28	178	0.7	0.00	0.00	543	1015	1353
Monte Burney	28	143	0.4	0.00	0.00	688	939	1123
Parque Nacionale Corcovado	41	380	11.3	0.03	0.02	1259	1536	1820
Parque Nacional Queulat	72	639	14.9	0.04	0.04	1391	1481	1547
Parque Nacional Vicente Perez Rosales	40	143	2.6	0.01	0.01	1896	2152	2617
Hornopiren	44	278	4.1	0.01	0.01	1301	1620	1793

Table 1. Glacier attributes per major region. Hmed is included as a proxy for ELA. In general ice thickness has an uncertainty of ± 11 % and volume has an uncertainty of ± 20 %.

The NPI and SPI have mean modelled ice thickness of 305 m ± 33.5 m and 331 m ± 36.4 m, respectively, and we find that four other major glacier regions, namely Cerro Hudson, Cerro Erasmo and Estrecho de Magallanes have mean modelled ice thicknesses > 100 m (Table 1). Maximum modelled ice thicknesses reaches 1315 m ± 144.6 m for the NPI and 1649 m ± 181.4 m for the SPI (Table 1). The total modelled volume of ice per major region is 4326.6 km^3 ± 865.3 km^3 for the SPI, 1234.6 km^3 ± 246.9 km^3 for the NPI and 151.9 km^3 ± 30.4 km^3 for Cordillera Darwin (Table 1). All other major glacier regions each contain a total of < 40 km^3 glacier ice (Table 1).

Our modelled ice thickness distribution, which is freely available as a downloadable ArcGIS-format 100 m grid raster via supplementary information, and a part of which is depicted in Figure 2B, can be compared with that derived from gravity measurements by Gourlet et al. (2016) on the NPI and on the northern part of the SPI. Our modelled subglacial bed topography has greater relief and complexity than that derived by Gourlet et al (2014) from airborne gravity surveys (Figure 4). Quantitatively, the mean 'measured-modelled' difference is 196 m, or ~ 18 % of ice thickness) along the transects presented by Gourlet et al. (Figure 4), but it must be noted that unfortunately their gravity survey lines do not correspond spatially to our centrelines. In more detail, their ice thickness on these transects is an interpolation between their gravity lines, (ii) they acknowledged error in narrow valleys and away from survey lines of > 100 m, and (iii) our ice thickness along these transects is an interpolation of that calculated along the centreline(s).

Profiles of bed topography along our centrelines are relatively bumpy in comparison to the estimated bed topography between them and a glacier margin where the interpolation produces a very smooth surface. This is a demonstration that our model has uncertainty in the centreline ice thickness calculation, and then more uncertainty in the spatial interpolation of ice thickness. In general therefore we suppose that our model reflects the general features and the orders of magnitude of ice thicknesses in a region, especially with relatively small glaciers, but the complex subglacial topography of the main icefields remains relatively crudely estimated.

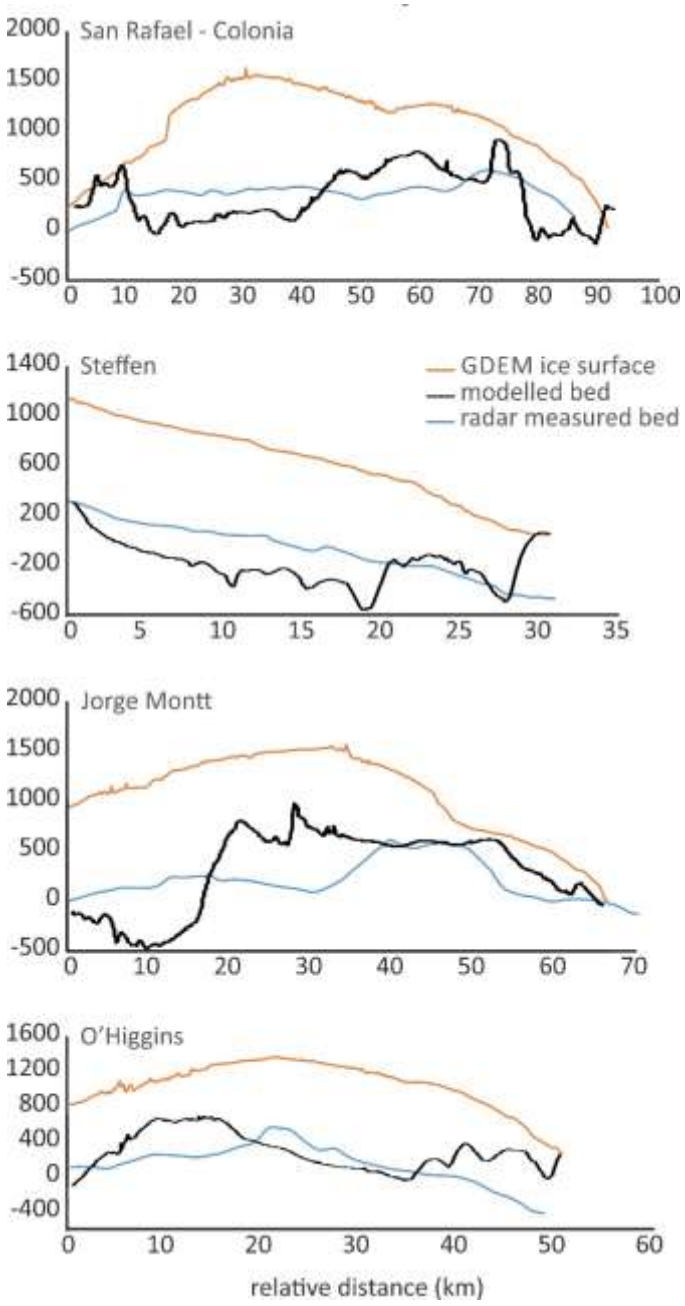

Figure 4: Comparison of our modelled bed topography along transects presented by Gourlet et al. (2016) who derived ice thickness from airborne gravity measurements. The position of these transects is depicted in our Fig. SI_B.

Nevertheless, our modelled bed topography identifies mountain ridges submerged beneath the ice, major troughs submerged beneath the ice, major overdeepenings and substantial areas with ice below sea level (Figure 2C). This character of the southern South America subglacial topography has been noted before by Gourlet et al. (2016) for parts of the NPI and SPI but here we are able to produce a bed topography map with complete coverage across the whole area occupied by the Patagonian Icefields. The total area with ice beneath sea level is modelled to be contained with 73 zones

encompassing a total area of 655 km^2, with a mean elevation of -34 m ± 4 m and with a total volume of 91.5 km^3 ± 18.3 km^3. The five largest of these subglacial areas below sea level are each > 40 km^2 and each > 4 km^3 and are beneath San Quintin and San Rafael on NPI, and beneath Jorge Montt, Occidental and Pio XI glaciers on the SPI. Other major glacier regions with bed elevations below zero are Gran Campo Nevado (total < 0.001 km^3), Cordillera Darwin (total 0.4 km^3), and Torres del Paine (total 0.05 km^3).

The total area of glacier ice within subglacial enclosed topographic basins, or overdeepenings, which are prime locations for meltwater retention and thus which affect ice dynamics (Cook and Swift, 2012) and represent possible (future) lakes, is modelled to be 1200 km^2. In total 282 individual overdeepenings are identified, with a mean depth of 38 m ± 4 m and a total volume (i.e. as if filled with water to the brim) of 101.7 km^3 ± 20 km^3. The five largest overdeepenings in terms of area and volume are all on the SPI on Jorge Montt, Occidental, O'Higgins, Viedma and Guilardi glaciers. These five overdeepenings each have a volume > 9 km^3. Other major regions with overdeepenings are the NPI (total 9.75 km^3), Gran Camp Nevado (0.065 km^3), Cerro Erasmo (0.18 km^3), Cerro Hudson (0.23 km^3), Cordillera Darwin (5. 46 km^3), El Condor (0.02 km^3) and Estrecho de Magallanes (0.085 km^2).

The maximum modelled depth of a single overdeepening is slightly > 400 m but the mean modelled depth of all overdeepenings is just 6.5 m. Overdeepenings with some part of their modelled depth > 300 m are restricted to Steffen and San Rafael on the NPI and these are 12 km^2 and 22 km^2 in area, respectively, although several other (areally) larger though shallower overdeepenings occur in both glaciers and beneath other NPI glaciers. On the SPI Jorge Montt, O'Higgins, Pio XI, Viedma, Guilardi and Tyndall glaciers all have overdepeenings with some part of their modelled depths > 300 m.

To consider potential future sea level rise (SLR) rather than total sea level equivalent (SLE), the volume of ice below sea level and potential lakes must be considered (c.f. Haeberli and Linsbauer, 2013). We calculate the SLR of southern South America glaciers per major region (Table 1) and to a total of 14.71 mm ± 2.94 mm, which is 2.5 % less than the SLE. Ice below sea level accounted for 74 % of this difference between SLE and SLR, and ice within overdeepenings, i.e. potential future lakes, accounted for 26 %.

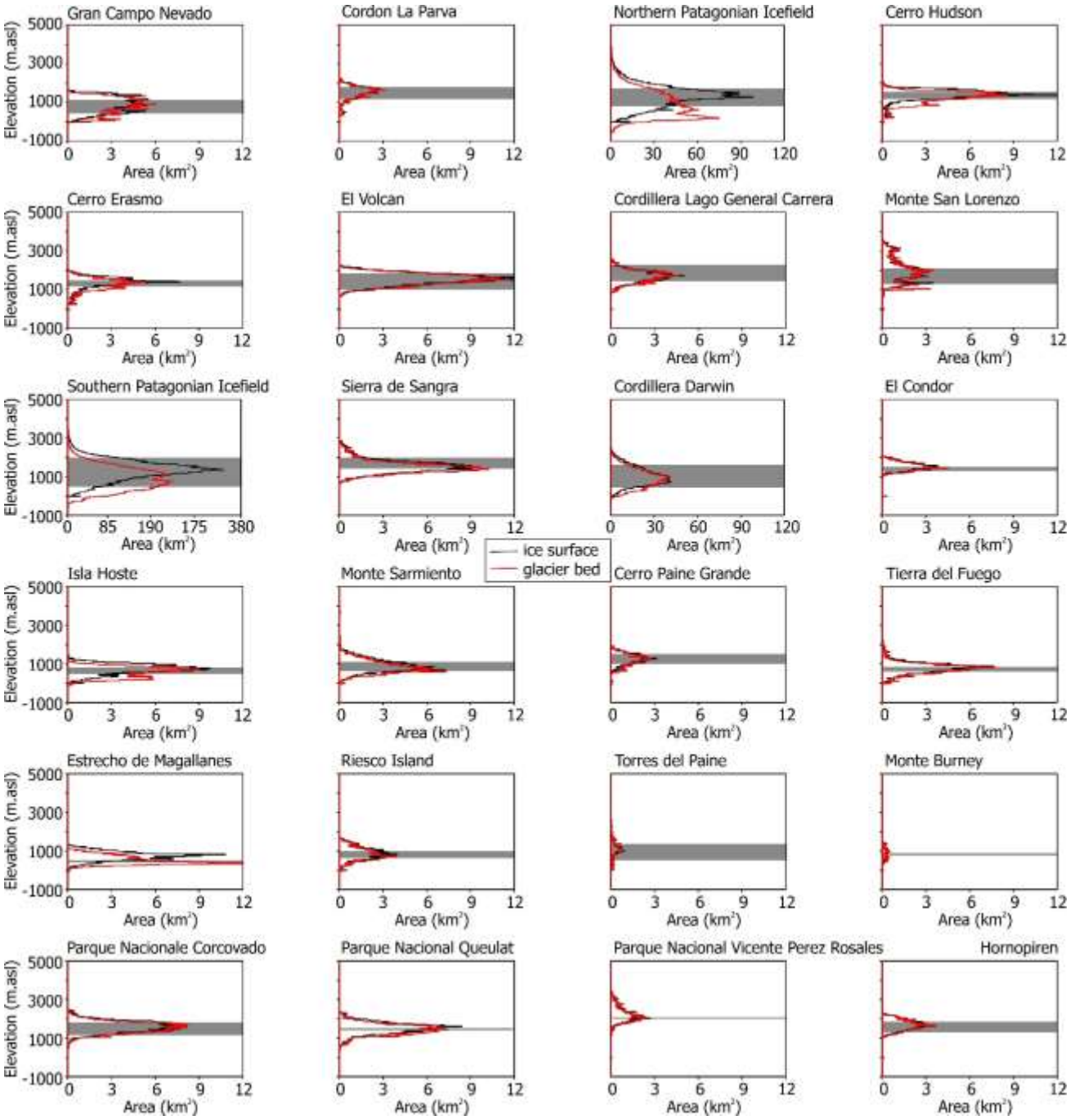

Figure 5. Ice surface (black line) and bed (red line) hypsometry for all 24 major glacier regions in southern South America. Note x-axis is different for Southern Patagonian Icefield, Northern Patagonian Icefield and Cordillera Darwin. Grey horizontal bar represents range of ELAs as estimated from Hmed of each glacier.

The spatial variation in the difference between SLE and SLR across southern South America (Table 1) is especially interesting because each region and indeed each individual glacier has a different climatic sensitivity / rates of recession (Davies and Glasser 2012; Gourlet et al. 2016). In a graphical manner the sensitivity to present climate and the consequences of possible future climatic changes (c.f. Raper and Braithwaite, 2009) on the glaciers of southern South America can be crudely

514 assessed. Glacier ice surface and subglacial bed elevation hypsometry is plotted per major region in
515 Figure 5, together with the range of Hmed values for all glaciers in that region as a proxy for ELA.
516 Most pertinently, these graphs indicate that large amounts of ice in the NPI, SPI, and to a lesser
517 extent in Gran Campo Nevado, Cerro Hudson, Cordillera Darwin, Isla Hoste and Estrecho de
518 Magallanes regions already lies well below Hmed and thus depend for survival on replenishment via
519 ice flux from glacier accumulation areas. However, the glaciated area situated attitudinally above the
520 range of Hmed per major region is proportionally high (> 20 % of all ice in the region) only for
521 Gran Campo Nevado, Monte San Lorenzo, El Condor, Isla Hoste, Tierra del Fuego, Estrecho de
522 Magallanes, Riesco Island, Monte Burney, Parque Nacional Queulat and Parque Nacional Vicente
523 Perez Rosales. These regions are all glaciers, ice caps and glaciated volcanoes outlying the major
524 (NPI and SPI) ice fields and the majority of them are in southern Patagonia. Clearly, a simple change
525 in ELA, such as a shift upwards in elevation by 100 m, will have dramatically spatially-differing
526 consequences for southern South America glaciers.
527
528 Analysis of the ice volume remaining within each major river catchment is an important concern for
529 water resources, including irrigation and hydropower, for example, especially given that southern
530 South America river flow records have exhibited a pronounced negative trend since the 1950s
531 (Masiokas et al., 2008). We find that only the Rio Chico and the Rio Santa Cruz catchments in
532 Argentina, and the Rio Chacabuco in Chile have modelled ice volumes > 300 km^3 (Figure 6). The
533 Rio Deseado and the Rio Coyle catchments have modelled ice volumes 193 km^3 ± 38 km^3 and 181
534 km^3 ± 36 km^3, respectively, and a few other smaller catchments on the western side of the NPI and
535 on the western side of the SPI each have ice volumes within them of < 100 km^3. The Rio Ibanez and
536 the Rio Simpson catchments in Chile have a modelled ice volume of 29 km^3 ± 6 km^3 and 24 km^3 ± 5
537 km^3, respectively. Except for a few small catchments at the southern end of the Cordillera Darwin
538 virtually all other river catchments across southern South America have modelled ice volumes < 10
539 km^3 (Figure 6). Where river catchments are large, but ice volumes are small and diminishing, river
540 flows must be progressively sustained by precipitation and any groundwater sources.
541
542

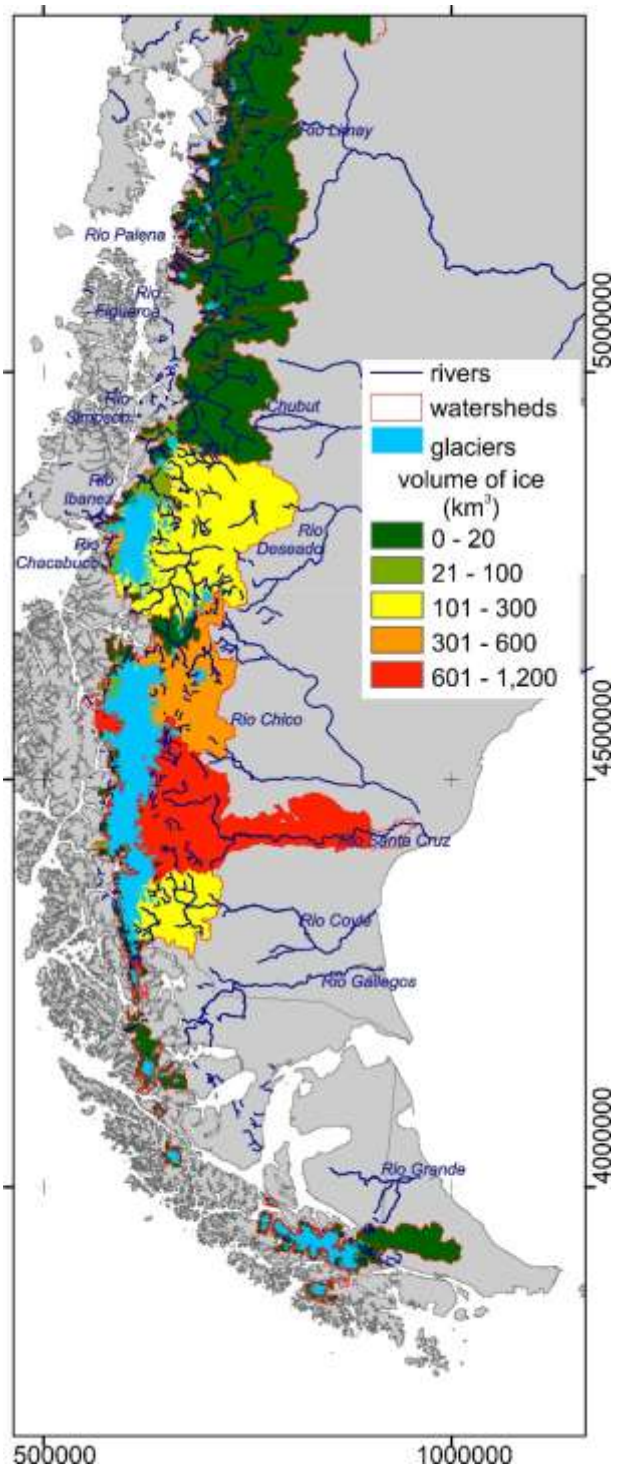

Figure 6. Total ice volume modelled for the major river catchments of Patagonia.

Discussion

Regional total sea level contributions

Huss and Farinotti (2012) used a physically-based approach to model ice thickness for Southern Andes glaciers (n = 19,089, area = 32,521 km^2) and reported a mean thickness of 205 m and a total

549 volume 6,674 ± 507 km^3. That mean thickness is slightly less than the mean thickness of 264 m
550 modelled in this study. Their total volume is 11 % more than our 5954.6 km^3 ± 1190.9 km^3, but both
551 estimates agree within their respective uncertainty, and the uncertainty of the Huss and Farinotti
552 model is ~ half that of our study. This suggests that whilst our study covers a smaller geographical
553 region because it uses the World Glacier Inventory (WGI)-GLIMS outlines whereas Huss and
554 Farinotti (2012) used the Randolph Glacier Inventory (RGI) outlines, it is apparently considering the
555 vast majority of ice volume. Furthermore, Huss and Farinotti (2013) reported a SLE of 16.6 ± 1.3
556 mm for Southern Andes glaciers, which can be compared to our 15.08 mm ± 3.01 mm and to our
557 SLR of 14.71 mm ± 2.9 mm. Furthermore, using Radic and Hock's (2011) projected SLE
558 contributions of South American glaciers from 2000 to 2100 of 0.01 $mm.yr^{-1}$, we calculate those
559 contributions would cause a reduction of 6.8 % of the total ice mass available over that time period.
560 For interest, further comparison of Radic and Hock's estimates of SLE with that of Huss and
561 Farinotti's and of the usage of the WGI-GLIMS glacier outlines versus those from the RGI has been
562 explored further by Grinstead (2013).
563
564 SLE contributions from southern South America glaciers are accelerating. Rignot et al. (2003)
565 reported rates of 0.042 ± 0.002 $mm.yr^{-1}$ for 1968/1975 to 2000, but rates of 0.105 ± 0.011 $mm.yr^{-1}$
566 for 1995 to 2000. For the time period 2000 to 2012 Willis et al. (2012) reported SLE contributions
567 from the SPI and the NPI combined of 0.067 ± 0.004 $mm.yr^{-1}$. These rates over recent decades are an
568 order of magnitude greater than that calculated over centennial scales since the Little Ice Age
569 (Glasser et al., 2011: 0.0018 $mm.yr^{-1}$ from NPI since 1870, and 0.0034 $mm.yr^{-1}$ from SPI since 1650).
570 The longer time to disappearance is produced using the most conservative SLE rate of Radic and
571 Hock (2011), which is a process-based estimation, whereas the other shorter times to disappearance
572 are simply via an extrapolation of modern rates and thus ignore probably future feedbacks between
573 glacier mass balance and ice dynamics. The range of these published estimates of SLE highlight the
574 need for future numerical modelling of southern South America glacier systems. The distributed ice
575 thickness and bed topography datasets produced by this study will be very useful for this future
576 modelling, and especially for examining any spatio-temporal variability in the response of glacier
577 dynamics to climate change.
578
579 ***Local topography and individual glacier dynamics***
580 Southern South America glacier changes in area and length since the Little Ice Age (LIA) have
581 considerable spatial heterogeneity (Davies and Glasser, 2012) and likely will do so in the future too.
582 Gourlet et al. (2016) recently discussed that local topography apparently exerts a much stronger

583 control on glacier response variability across southern South America than regional climate gradients
584 (see regional ELA mapped in SI_A). In this study we found it crucial to include nunataks in our
585 glacier outlines so as to delimit ice-free parts within glacier drainage basins to which ice thickness
586 should be interpolated to zero. Glaciers with termini that are retreating into overdeepened basins
587 such as Jorge Montt, Occidental, O'Higgins, Viedma and Guilardi, Steffen, Colonia and Tyndall,
588 could (i) store large amounts of meltwater subglacially with the potential for glacier outburst floods,
589 or 'jökulhlaups', and (ii) become lacustrine-terminating if not already with implications for ice
590 dynamics as well as for meltwater and sediment fluxes (Carrivick and Tweed, 2013; Loriaux and
591 Casassa, 2013). The numerous southern South America glaciers that presently terminate in the sea, a
592 tidal lagoon or a freshwater lake are subject to subaqueous melting and tidally-induced longitudinal
593 stresses (Truffer and Motyka, 2016). Our model poorly represents these tidewater glaciers due to
594 their floating termini. Glaciers with large zones of subglacial elevations below sea level will increase
595 in surface gradient and thus likely accelerate in velocity with ongoing terminus retreat.
596
597 Finally, whilst some southern South America glaciers are within semi-arid regions, many are located
598 in regions with steep topographic gradients and high precipitation rates and they have snow and firn
599 contributing to volumes (if determined geodetically) and accumulation enhanced by avalanching and
600 snow drift. Glaciers in these 'wet' conditions can be relatively insensitive to increasing air
601 temperatures, as has been modelled for Swiss glaciers (Huss and Fischer, 2016) and identified for an
602 Austrian glacier (Carrivick et al., 2015) and for glaciers in the Canadian Rockies (Debeer and Sharp,
603 2009). These spatio-temporal sensitivities of southern South America glaciers to air temperature and
604 to precipitation changes mean that projection of future hydrograph patterns per major river
605 catchment will need consideration of not only ice surface but also subglacial hypsometry, as
606 provided by this study, in relation to present and projected glacier ELAs.
607
608 **Conclusions and future work**
609 This first complete coverage of modelled distributed ice thickness, which we make freely available
610 as (i) an ArcGIS-format raster and (ii) a table of attributes per glacier (supplementary information)
611 across the whole of southern South America greatly extends in coverage and spatial detail the few
612 tens of available ice thickness point measurements in South America (Gärtner-Roer et al., 2014) and
613 the gravity measurements coverage of parts of the ice thickness of the NPI and SPI (Gourlet et al.,
614 2016). This first-order ice thickness modelling has in turn permitted modelling of bed topography
615 and of ice volume per glacier, per major glacier region and for southern South America in total. The
616 total ice volume of southern South America is 5955 km^3 ± 1191 km^3 and this volume equates to

5458.3 Gt ± 1091.6 Gt ice and to 15.08 mm ± 3.01 mm sea level equivalent (SLE). Accounting for bed elevations below sea level and overdeepenings that will likely store future meltwater, the maximum potential sea level rise (SLR) from all southern South America glaciers is 14.71 mm ± 2.9 mm. However, the rate at which individual glaciers will lose mass in the future depends on complex feedbacks between glacier dynamics and local topography, glacier hypsometry and regional and local ELAs and this study has produced those datasets.

Development of the estimates of ice thickness presented herein could focus firstly on derivation of glacier flow lines rather than relying on relatively sparse centrelines, and should consider a routine for better-representing floating glacier terminii. Future studies could readily utilise the datasets produced in this study in volume-area scaling (Bahr et al., 1997, 2014) and also volume-thickness scaling and other area- and slope-dependant models (see Gärtner-Roer et al., 2014 for application of these). In addition to V-A scaling, the parameters of altitude range-area, mean glacier thickness and altitude range can be used for ice volume sensitivity analysis (c.f. Raper and Braithwaite, 2009), although some consideration of mass balance gradient has yet to be worked out for all southern South America glaciers. Future work on numerical process-based glacier mass balance modelling will require distributed bed topography and ice thickness and is necessary to unravel the complex feedbacks and process-links between glacier mass balance, glacier dynamics and tidewater and lacustrine influences on glacier dynamics. The bed topography and especially the realisation of large zones of subglacial elevations below sea level and the large zones of overdeepenings are important for glacier or ice sheet models and for glacial isostatic adjustment models. They are also of concern for potential future meltwater retention and thus for consideration of water resources and glacier hazards.

Acknowledgements

Development of the perfect-plasticity model was supported by a NERC PhD studentship (NE/K500847/1) to WJ.

649

650 **References**

651 Ackert, R.P., Becker, R.A., Singer, B.S., Kurz, M.D., Caffee, M.W., Mickelson, D.M., 2008.
652 Patagonian glacier response during the late glacial-Holocene transition. Science 321, 392-395.

653 Anacona, P.I., Norton, K., Mackintosh, A., 2014. Moraine-dammed lake failures in Patagonia and
654 assessment of outburst susceptibility in the Baker Basin. Nat. Hazards Earth Syst. Sci 14, 3243-3259.

655 Aravena, J.C., Luckman, B.H., 2009. Spatio-temporal rainfall patterns in Southern South America.
656 International Journal of Climatology 29, 2106-2120.

657 Barcaza, G., Aniya, M., Matsumoto, T., Aoki, T., 2009. Satellite-derived equilibrium lines in
658 Northern Patagonia Icefield, Chile, and their implications to glacier variations. Arctic, Antarctic, and
659 Alpine Research 41, 174-182.

660 Bahr, D. B., Meier, M. F., & Peckham, S. D. (1997). The physical basis of glacier volume-area
661 scaling. Journal of Geophysical Research: Solid Earth, 102(B9), 20355-20362.

662 Bahr, D.B., Pfeffer, W.T., Kaser, G., 2014. A Review of Volume-Area Scaling of Glaciers. Reviews
663 of Geophysics.

664 Boex, J., Fogwill, C., Harrison, S., Glasser, N.F., Hein, A., Schnabel, C., Xu, S., 2013. Rapid
665 thinning of the late Pleistocene Patagonian Ice Sheet followed migration of the Southern Westerlies.
666 Scientific Reports 3, 1-6.

667 Bown, F., Rivera, A., Zenteno, P., Bravo, C., Cawkwell, F., 2014. First Glacier Inventory and Recent
668 Glacier Variation on Isla Grande de Tierra Del Fuego and Adjacent Islands in Southern Chile. In
669 Global Land Ice Measurements from Space (pp. 661-674). Springer Berlin Heidelberg.

670 Braithwaite, R.J., Raper, S.C.B., 2002. Glaciers and their contribution to sea level change. Physics
671 and Chemistry of the Earth, Parts A/B/C 27, 1445-1454.

672 Braithwaite, R. J., & Raper, S. C. B. (2010). Estimating equilibrium-line altitude (ELA) from glacier
673 inventory data. Annals of Glaciology, 50(53), 127-132.

674 Carrasco, J., Casassa, G., Rivera, A., 2002. Meteorological and climatological aspect of the Southern
675 Patagonian Icefield, In: Casassa, G., Sepulveda, F.V., Sinclair, R.M. (Eds.), The Patagonian
676 Icefields. Kluwer-Plenum, New York, pp. 29-41.

677 Carrivick, J. L., Berry, K., Geilhausen, M., James, W. H., Williams, C., Brown, L. E., (2015).
678 Decadal-scale changes of the Ödenwinkelkees, Central Austria, suggest increasing control of
679 topography and evolution towards steady state. Geografiska Annaler Series A Physical Geography
680 97, 543–562.

681 Carrivick, J. L., & Tweed, F. S. (2013). Proglacial lakes: character, behaviour and geological
682 importance. Quaternary Science Reviews, 78, 34-52.

683 Casassa, G., 1987. Ice thickness deduced from gravity anomalies on Soler Glacier, Nef Glacier and
684 the Northern Patagonia Icefield. Bulletin of glacier research, 43-57.

685 Casassa, G., Rivera, A., Aniya, M., Naruse, R., 2002. Current knowledge of the Southern Patagonia
686 Icefield.

687 Cook, S. J., & Swift, D. A. (2012). Subglacial basins: Their origin and importance in glacial systems
688 and landscapes. Earth-Science Reviews, 115(4), 332-372.

689 Cuffey, K. M., & Paterson, W. S. B., 2010. The physics of glaciers. Academic Press.

690 Davies, B.J., Glasser, N.F., 2012. Accelerating recession in Patagonian glaciers from the "Little Ice
691 Age" (c. AD 1870) to 2011. Journal of Glaciology 58, 1063-1084.

692 De Angelis, H., 2014. Hypsometry and sensitivity of the mass balance to changes in equilibrium-line
693 altitude: the case of the Southern Patagonia Icefield. Journal of Glaciology 60, 14-28.

694 Debeer, C. M., and Sharp, M. J. (2009). Topographic influences on recent changes of very small
695 glaciers in the Monashee Mountains, British Columbia, Canada. Journal of Glaciology 55, 691–700.

696 Driedger, C. and P. Kennard. 1986a. Glacier volume estimation on Cascade volcanoes: an analysis
697 and comparison with other methods. Annals of Glaciology 8, 59-64.

698 Driedger, C. L. and P. M. Kennard. 1986b. Ice volumes on Cascade volcanoes: Mount Rainier,
699 Mount Hood, Three Sisters, and Mount Shasta. Washington: U.S. Geological Survey Professional
700 Paper 1365

701 Dussaillant, A., Benito, G., Buytaert, W., Carling, P., Meier, C., Espinoza, F., 2009. Repeated
702 glacial-lake outburst floods in Patagonia: an increasing hazard? Natural Hazards 54, 469-481.

703 Farinotti, D. and M. Huss. 2013. An upper-bound estimate for the accuracy of glacier volume–area
704 scaling. The Cryosphere, 7(6), pp.1707-1720.

705 Farinotti, D. et al. 2009. A method to estimate the ice volume and ice-thickness distribution of alpine
706 glaciers. Journal of Glaciology, 55(191), pp.422-430.

707 Fischer, A. and M. Kuhn. 2013. Ground-penetrating radar measurements of 64 Austrian glaciers
708 between 1995 and 2010. Annals of Glaciology, 54(64), pp.179-188.

709 Gardner, A.S., Moholdt, G., Cogley, J.G., Wouters, B., Arendt, A.A., Wahr, J., Berthier, E., Hock,
710 R., Pfeffer, W.T., Kaser, G., Ligtenberg, S.R.M., Bolch, T., Sharp, M.J., Hagen, J.O., van den
711 Broeke, M.R., Paul, F., 2013. A Reconciled Estimate of Glacier Contributions to Sea Level Rise:
712 2003 to 2009. Science 340, 852-857.

713 Gärtner-Roer, I., Naegeli, K., Huss, M., Knecht, T., Machguth, H., & Zemp, M. (2014). A database
714 of worldwide glacier thickness observations. Global and Planetary Change, 122, 330-344.

715 Garreaud, R., Lopez, P., Minvielle, M., Rojas, M., 2013. Large-Scale Control on the Patagonian
716 Climate. Journal of Climate 26, 215-230.

Garreaud, R.D., Vuille, M., Compagnucci, R., Marengo, J., 2009. Present-day South American climate. Palaeogeography Palaeoclimatology Palaeoecology 281, 180-195.

Glasser, N.F., Harrison, S., Jansson, K.N., Anderson, K., Cowley, A., 2011. Global sea-level contribution from the Patagonian Icefields since the Little Ice Age maximum. Nature Geoscience 4, 303-307.

Godoi, M. A., Shiraiwa, T., Kohshima, S., & Kubota, K. (2002). Firn-core drilling operation at Tyndall glacier, Southern Patagonia Icefield. In The Patagonian Icefields (pp. 149-156). Springer US.

Gourlet, P., Rignot, E., Rivera, A., Casassa, G., 2016. Ice thickness of the northern half of the Patagonia Icefields of South America from high-resolution airborne gravity surveys. Geophysical Research Letters 43, 241-249.

Grinsted, A., 2013. An estimate of global glacier volume. The Cryosphere 7, 141-151.

Haeberli, W. and M. Hoelzle. 1995. Application of inventory data for estimating characteristics of and regional climate-change effects on mountain glaciers: A pilot study with the European Alps. Annals of Glaciology, 21, pp.206-212.

Haeberli, W., & Linsbauer, A. (2013). Brief communication" Global glacier volumes and sea level–small but systematic effects of ice below the surface of the ocean and of new local lakes on land". The Cryosphere, 7(3), 817-821.

Harrison, S., Glasser, N., Winchester, V., Haresign, E., Warren, C., Jansson, K., 2006. A glacial lake outburst flood associated with recent mountain glacier retreat, Patagonian Andes. The Holocene 16, 611-620.

Hess, H., 1893: Über die Grenze zwischen Schmelz und Sammelgebiet der Gletscher. Verhanlungen der Gesellschaft Deutscher Naturfreunde und Ärzte, Nürnberg.

Hoelzle, M. et al. 2007. The application of glacier inventory data for estimating past climate change effects on mountain glaciers: A comparison between the European Alps and the Southern Alps of New Zealand. Global and Planetary Change, 56(1), pp.69-82.

Huss, M., & Farinotti, D. (2012). Distributed ice thickness and volume of all glaciers around the globe. Journal of Geophysical Research: Earth Surface, 117(F4).

Huss, M., & Fischer, M. (2016). Sensitivity of very small glaciers in the Swiss Alps to future climate change. Frontiers in Earth Science, 4, 34.

Hutchinson, M. 1989. A new procedure for gridding elevation and stream line data with automatic removal of spurious pits. Journal of Hydrology, 106(3), pp.211-232.

Huybrechts, P., 2007. Ice sheet modeling. in: B. Riffenburgh (ed): Encyclopedia of the Antarctic, Routledge, New York and London, 514-517.

751 Ivins, E.R., Watkins, M.M., Yuan, D.-N., Dietrich, R., Casassa, G., Rülke, A., 2011. On-land ice loss
752 and glacial isostatic adjustment at the Drake Passage: 2003-2009. J. Geophys. Res. 116, B02403.

753 Jaber, W. A., Floricioiu, D., & Rott, H. (2014, July). Glacier dynamics of the Northern Patagonia
754 Icefield derived from SRTM, TanDEM-X and TerraSAR-X data. In Geoscience and Remote Sensing
755 Symposium (IGARSS), 2014 IEEE International (pp. 4018-4021). IEEE.

756 Jacob, T., Wahr, J., Pfeffer, W. T., & Swenson, S. (2012). Recent contributions of glaciers and ice
757 caps to sea level rise. Nature, 482(7386), 514-518.

758 James, W. H., Carrivick, J. L., 2016. Automated modelling of spatially-distributed glacier ice
759 thickness and volume. Computers & Geosciences 92, 90-103.

760 Kerr, A., Sugden, D.E., 1994. The sensitivity of the south Chilean snowline to climatic change.
761 Climate change 28, 255-272.

762 Koppes, M., Conway, H., Rasmussen, L.A., Chernos, M., 2011. Deriving mass balance and calving
763 variations from reanalysis data and sparse observations, Glaciar San Rafael, northern Patagonia,
764 1950-2005. The Cryosphere 5, 791-808.

765 Lehner, B., Verdin, K., Jarvis, A. (2006): HydroSHEDS Technical Documentation. World Wildlife
766 Fund US, Washington, DC. Available at http://hydrosheds.cr.usgs.gov.

767 Lamy, F., Kilian, R., Arz, H.W., Francois, J.-P., Kaiser, J., Prange, M., Steinke, T., 2010. Holocene
768 changes in the position and intensity of the southern westerly wind belt. Nature Geoscience 3, 695-
769 699.

770 Levermann, A., Clark, P.U., Marzeion, B., Milne, G.A., Pollard, D., Radic, V., Robinson, A., 2013.
771 The multimillennial sea-level commitment of global warming. Proceedings of the National Academy
772 of Sciences 110, 13745-13750.

773 Li, H. et al. 2012. An extended "perfect-plasticity" method for estimating ice thickness along the
774 flow line of mountain glaciers. Journal of Geophysical Research-Earth Surface, 117(F01020).

775 Linsbauer, A., F. Paul and W. Haeberli. 2012. Modeling glacier thickness distribution and bed
776 topography over entire mountain ranges with GlabTop: Application of a fast and robust approach.
777 Journal of Geophysical Research, 117(F3).

778 Linsbauer, A. et al. 2009. The Swiss Alps without glaciers – a GIS-based modelling approach for
779 reconstruction of glacier beds. In: Proceedings of Geomorphometry 2009, Zurich, Switzerland.

780 Loriaux, T., Casassa, G., 2013. Evolution of glacial lakes from the Northern Patagonia Icefield and
781 terrestrial water storage in a sea-level rise context. Global and Planetary Change 102, 33-40.

782 Masiokas, M. H., Villalba, R., Luckman, B. H., Lascano, M. E., Delgado, S., & Stepanek, P. (2008).
783 20th-century glacier recession and regional hydroclimatic changes in northwestern Patagonia. Global
784 and Planetary Change, 60(1), 85-100.

Mernild, S.H., Beckerman, A.P., Yde, J.C., Hanna, E., Malmros, J.K., Wilson, R., Zemp, M., 2015. Mass loss and imbalance of glaciers along the Andes Cordillera to the sub-Antarctic islands. Global and Planetary Change 133, 109-119.

Moreno, P.I., Villa-Martínez, R., Cárdenas, M.L., Sagredo, E.A., 2012. Deglacial changes of the southern margin of the southern westerly winds revealed by terrestrial records from SW Patagonia (52°S). Quaternary Science Reviews 41, 1-21.

Mouginot, J., Rignot, E., 2015. Ice motion of the Patagonian Icefields of South America: 1984-2014. Geophysical Research Letters, 2014GL062661.

Nye, J. 1965. The flow of a glacier in a channel of rectangular, elliptic or parabolic cross-section. Journal of Glaciology, 5, pp.661-690.

Oerlemans, J., Fortuin, J.P.F., 1992. Sensitivity of Glaciers and Small Ice Caps to Greenhouse Warming. Science 258, 115-117.

Paterson, W. S. B. 1994. The physics of glaciers. 3rd ed. Oxford: Pergamon.

Paul, F., Mölg, N., 2014. Hasty retreat of glaciers in northern Patagonia from 1985-2011. Journal of Glaciology 60, 1033-1043.

Radić, V., & Hock, R. (2011). Regionally differentiated contribution of mountain glaciers and ice caps to future sea-level rise. Nature Geoscience, 4(2), 91-94.

Radic, V., Hock, R., Oerlemans, J., 2008. Analysis of scaling methods in deriving future volume evolutions of valley glaciers. Journal of Glaciology 54, 601-612.

Raper, S. C., & Braithwaite, R. J. (2009). Glacier volume response time and its links to climate and topography based on a conceptual model of glacier hypsometry. The Cryosphere, 3(2), 183-194.

Rasmussen, L.A., Conway, H., Raymond, C.F., 2007. Influence of upper air conditions on the Patagonia icefields. Global and Planetary Change 59, 203-216.

Raymond, C., Neumann, T.A., Rignot, E., Echelmeyer, K., Rivera, A., Casassa, G., 2005. Retreat of Glaciar Tyndall, Patagonia, over the last half-century. Journal of Glaciology 51, 239-247.

Rignot, E., Rivera, A., Casassa, G., 2003. Contribution of the Patagonia Icefields of South America to sea level rise. Science 302, 434-437.

Rivera, A., Casassa, G., 2002. Ice Thickness Measurements on the Southern Patagonia Icefield, In: Casassa, G., Sepulveda, F.V., Sinclair, H.D. (Eds.), The Patagonian Icefields. Springer US, pp. 101-115.

Rivera, A., Bown, F., 2013. Recent glacier variations on active ice capped volcanoes in the Southern Volcanic Zone (37°–46°S), Chilean Andes, Journal of South American Earth Sciences 45, 345-356.

Rivera, A., Benham, T., Casassa, G., Bamber, J., Dowdeswell, J.A., 2007. Ice elevation and areal changes of glaciers from the Northern Patagonia Icefield, Chile. Global and Planetary Change 59, 126-137.

Rivera, A., Corripio, J., Bravo, C., Cisternas, S., 2012. Glaciar Jorge Montt (Chilean Patagonia) dynamics derived from photos obtained by fixed cameras and satellite image feature tracking. Annals of Glaciology 53, 147-155.

Rott, H., Stuefer, M., Siegel, A., Skvarca, P., Eckstaller, A., 1998. Mass fluxes and dynamics of Moreno Glacier, Southern Patagonia Icefield. Geophysical Research Letters 25, 1407-1410.

Schaefer, M., Machguth, H., Falvey, M., Casassa, G., Rignot, E., 2015. Quantifying mass balance processes on the Southern Patagonia Icefield. The Cryosphere 9, 25-35.

Schneider, C., Schnirch, M., Acuña, C., Casassa, G., Kilian, R., 2007. Glacier inventory of the Gran Campo Nevado Ice Cap in the Southern Andes and glacier changes observed during recent decades. Global and Planetary Change 59, 87-100.

Schwikowski, M., Schläppi, M., Santibañez, P., Rivera, A., & Casassa, G. (2013). Net accumulation rates derived from ice core stable isotope records of Pío XI glacier, Southern Patagonia Icefield.

Truffer, M., Motyka, R., 2016. Where glaciers meet water: Subaqueous melt and its relevance to glaciers in various settings. Reviews of Geophysics 54, 220–239.

Warren, C. R., Sugden, D. E., 1993. The Patagonian Icefields: a glaciological review. Arctic and Alpine Research 25, 316-331.

Willis, M.J., Melkonian, A.K., Pritchard, M.E., Ramage, J.M., 2011. Ice loss rates at the Northern Patagonian Icefield derived using a decade of satellite remote sensing. Remote Sensing of Environment 117, 184-198.

Willis, M.J., Melkonian, A.K., Pritchard, M.E., Rivera, A., 2012. Ice loss from the Southern Patagonian Ice Field, South America, between 2000 and 2012. Geophys. Res. Lett. 39, L17501.

Supplementary Information

Figure SI_A. Glacier ELAs of the NPI (A), northern SPI (B) and southern SPI (C), highlighting discrepancy that tends to increase southwards between ELA modelled 1970 to 1990 from zero degree Celsius isotherm by Condom et al. (2007) and contemporary ELA as estimated by Hmed.

Figure SI_B. Subglacial bed elevation for NPI (A), northern SPI (B) and southern SPI (C) coloured to emphasise those areas below sea level and major overdeepenings.

SI_Table1. Attributes of elevation, ELA, ice thickness and volume for 617 individual Patagonian glaciers.

SI_Dataset Ice thickness ArcGIS format raster grid in UTM zone 18S projection.

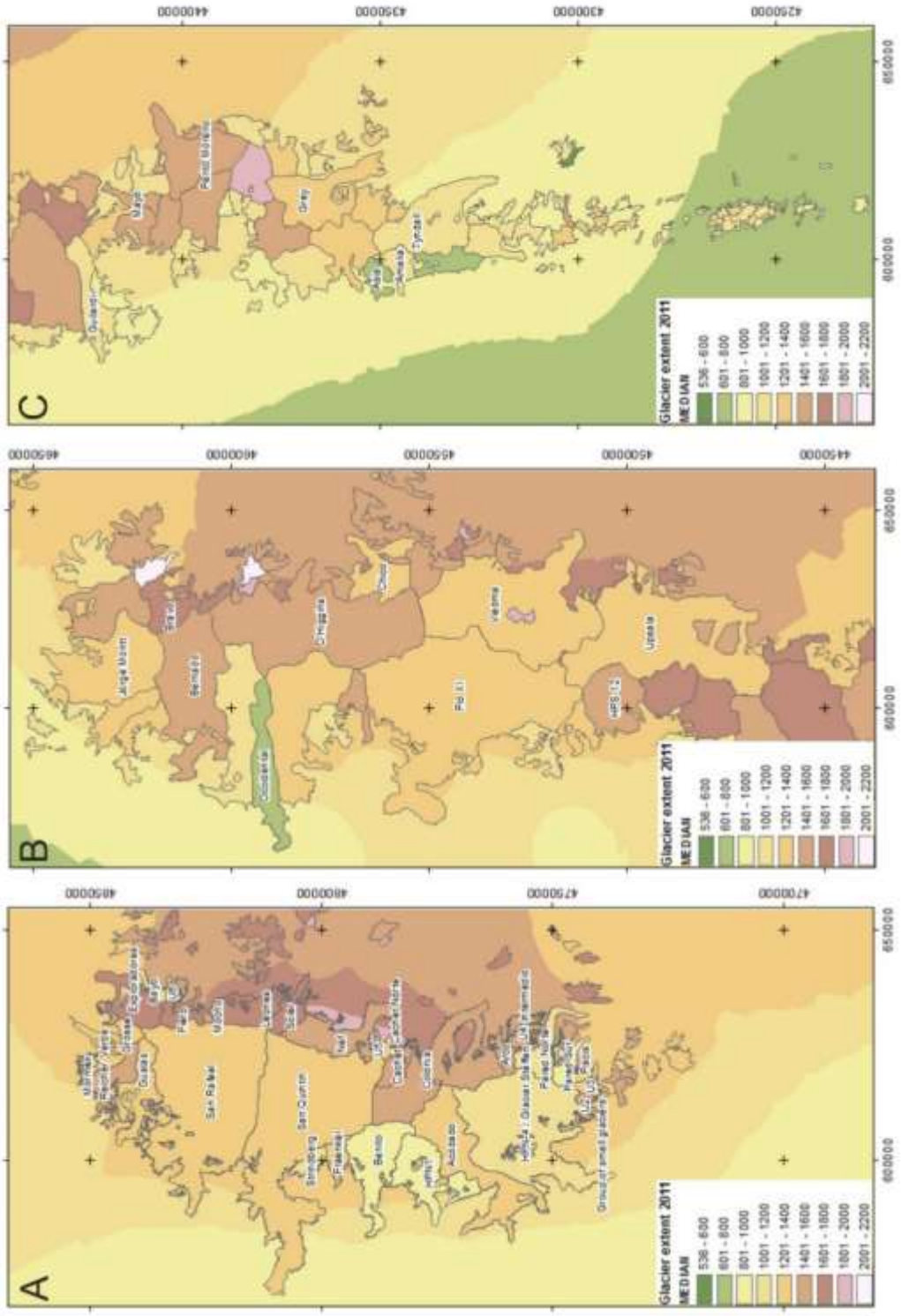

Figure SI_A. Glacier ELAs of the NPI (A), northern SPI (B) and southern SPI (C), highlighting discrepancy that tends to increase southwards between ELA modelled 1970 to 1990 from zero degree Celsius isotherm by Condom et al. (2007) and contemporary ELA as estimated by Hmed. Thus the greater differences in colours between glaciers and the surrounding region, the more out of balance that glacier geometry might be interpreted to be with regional climate. Adjacent glaciers with differing Hmeds can be interpreted to represent differing response times as glaciers adjust to climate change due to local scale effects such as wind-blown snow inputs to mass balance, avalanching and topographic shading to direct shortwave radiation, for example.

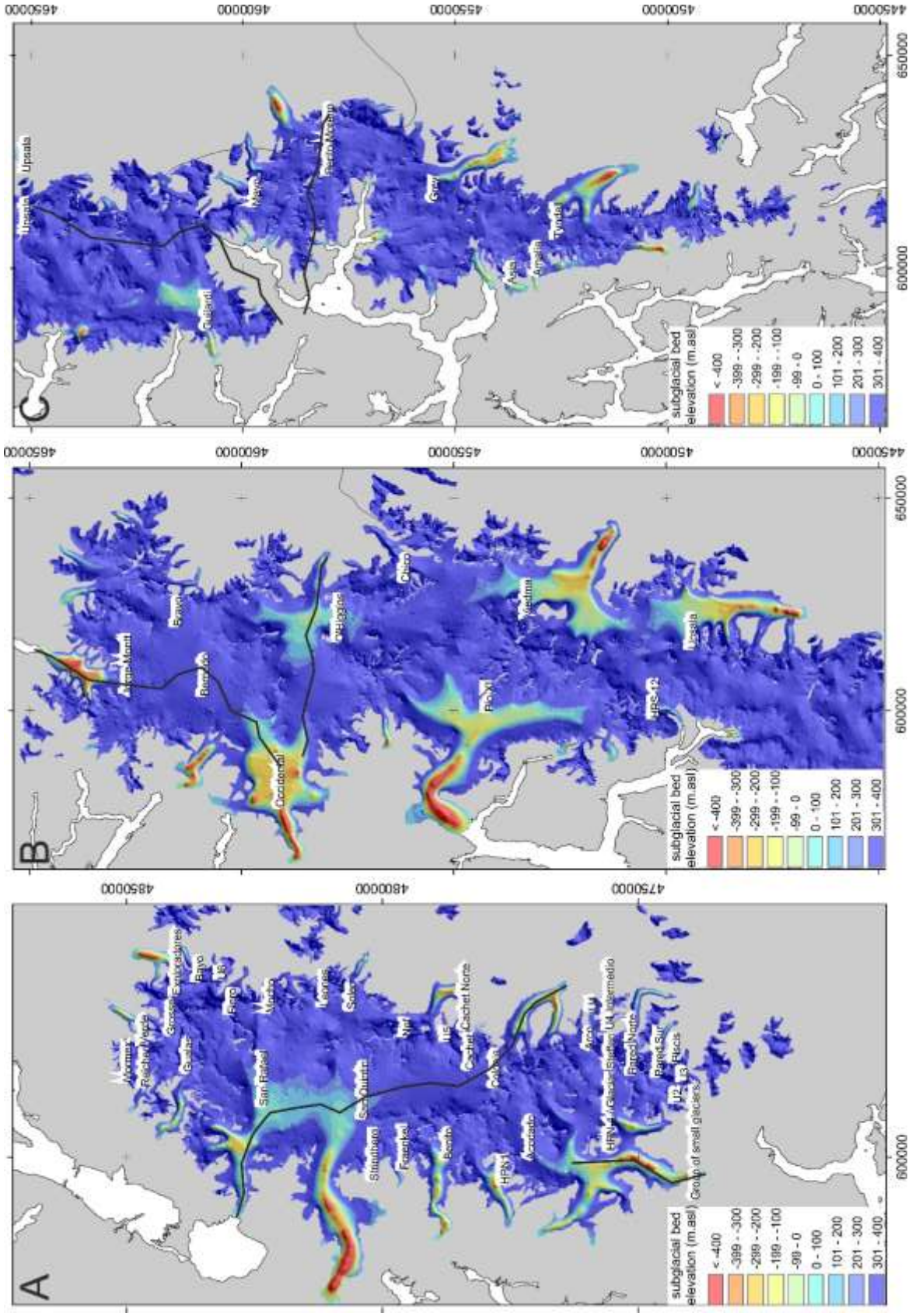

Figure SI_B. Subglacial bed elevation for NPI (A), northern SPI (B) and southern SPI (C) coloured to emphasise those areas below sea level and major overdeepenings. The black lines mark transects depicted in figure 4.